

HumanIBR: High Quality Image-based Rendering of Challenging Human Performers using Sparse Views

Tiansong Zhou, Tao Yu, Ruizhi Shao, Kun Li

Abstract—In this paper, we introduce HumanIBR, a method that addresses the challenge of novel view rendering of human performers that wear clothes with complex patterns using a sparse set of camera views. Some recent works have achieved remarkable rendering quality on humans that wear pure clothes using sparse views, but if the clothes have complex color patterns, the rendering quality is still very low. To this end, the proposed HumanIBR uses a human reconstruction net with pixel-aligned spatial transformer and a render net that uses geometry-guided pixel-wise feature integration to achieve to goal of high quality human reconstruction and rendering. The designed pixel-aligned spatial transformer calculates the correlations between the input views, producing human reconstruction results with high-frequency details presented in the input views. Based on the reconstruction, the geometry-guided pixel-wise visibility reasoning provides a guidance for multi-view feature integration, enabling the render net to render high quality images on novel views. Unlike previous neural rendering works that always need to train or fine-tune a separate network for each scene or human, our method is a general framework that is able to generalize to novel humans. Experiments show that our approach outperforms all the prior general or human-specific works on both synthetic data and real-world data.

Index Terms—Image-based rendering, neural rendering, human reconstruction, 3D vision



1 INTRODUCTION

Realistic free-viewpoint rendering of human performers is in increasing demand with the development of AR/VR and Image-Based Rendering (IBR) is a promising way that can render realistic images on novel views. However, current IBR methods [1], [2], [3], [4] always need to warp the input views to the novel views, which means they will rely on dense views as input. If only a sparse set of camera views is available, the performances of these warping-based methods will degrade dramatically as the wide camera baselines will cause severe occlusion problems.

To render human performers from sparse views, neural body [5] presents an implicit neural representation of dynamic humans. They anchor a latent code on each vertex of SMPL model [6] to integrate the observations over video frames. However, when the human performers wear clothes with complex color patterns or wear loose clothes such as long dresses, the rendering quality of [5] will be very low as the SMPL model does not contain any geometry details, which is not suitable for the rendering of loose clothes or complex clothes. Moreover, [5] needs to train a separate network for each human and the training procedure is extremely time-consuming (at least 10 hours for each human), which further limits its applications. Some works [7], [8] also seek to use a general model to render novel views from sparse views. But the rendering quality of these works will be very low without any fine-tuning.

In this work, we propose HumanIBR, a general method that is able to render high quality human images using sparse views. The used camera views are no more than 8 views in a uniformly distributed circle arrangement. To our knowledge, it is the first work that can take into considera-



Fig. 1. High quality reconstruction and rendering of a challenging human that wears long dress with complex patterns from only 6 input views, without any fine-tuning.

tion of sparsity, generalization and high quality rendering at the same time. Besides, we do not use any human geometry prior such as SMPL, so we can handle the human cases that wear loose clothes, such as long dress. An illustration is shown in Fig.1. Table 1 summarizes the key aspects of our approach relative to prior works.

To achieve the goal of high quality rendering from sparse views, the core is to solve the severe occlusion problems caused by the sparsity of input views. If we warp all the pixels of source views to the novel view, the render results will suffer severe artifacts and blurring as many pixels or areas are invisible in the novel view. For this end, we propose geometry-guided pixel-wise feature integration to map the source views to the novel view. We will perform visibility reasoning and find the visible source views for each pixel of the novel view, which will provide a guidance

TABLE 1

A comparison with prior works. Compared with prior works, our work is a general method that can render high quality images using sparse views.

	Sparsity?	General?	High quality?
Neural body [5]	✓	✗	✗
pixelNerf [8]	✓	✓	✗
IBRNet [7]	✓	✓	✗
Soft3D [2]	✗	✓	✓
Deep blending [1]	✗	✗	✓
Ours	✓	✓	✓

for the following feature integration.

For efficient visibility reasoning, a high quality reconstruction is essential. If the reconstruction results lose the geometry details that observed in the source views, the visibility reasoning will be inaccurate, resulting in rendering artifacts and blurring. Therefore, we present a pixel-aligned spatial transformer for multi-view feature fusion in the reconstruction net. The proposed transformer is able to preserve geometry details such as clothing folds that observed in the input views, resulting in highly-detailed reconstruction.

Unlike most of the neural-network-based rendering works that always need to train or fine-tune a separate network for each scene or human [5], [9], [10], the proposed HumanIBR is a general rendering framework. Benefit from the generalization ability of pixel-aligned spatial transformer and geometry-guided feature integration, our method is able to perform high quality reconstruction and rendering for unseen humans without any fine-tuning. Experiments show that our general approach significantly improves the rendering quality compared with all the existing general and scene/human-specific works. In summary, our contributions are:

- We propose a new general neural rendering framework capable of rendering novel views of human performers that wear clothes with complex patterns or loose clothes from a sparse set of camera views.
- A pixel-aligned spatial transformer that is able to perform efficient feature fusion in human reconstruction, enabling us to reconstruct highly detailed human models from sparse views.
- A geometry-guided pixel-wise feature integration method for efficiently solving the severe occlusion problems that caused by the sparsity of input views.
- We demonstrate significant rendering quality improvements of our method compared to the prior works, especially for humans that wear loose clothes or complex clothes.

2 RELATED WORK

Human Reconstruction. Human reconstruction has a long and overlapping history in both computer vision and graphics. In earlier years, multi-view stereo (MVS) is the most widely used method for human reconstruction. [11] proposes a continuous a depth map estimation method for

improving the performances of MVS. Over the past decade, benefit from the development of hardware, many works [12], [13], [14], [15] take single or multi RGBD views as input to get amazing real-time high fidelity human reconstruction and rendering. However, the relied depth sensors are only able to capture humans or objects that are near the sensors. When humans move far from the sensors (farther than 3m), the depth sensors will fail capturing depth streams, which greatly limits their applications. In recent years, one of the most promising research directions for human reconstruction is pixel-aligned implicit function (PIFu) [16]. PIFu takes a single color image as input and encode the image to generate pixel-aligned image features. Based on the pixel-aligned features that contain the geometry details in the input image, they learns an implicit function over the 3D space. Following PIFu, PIFuHD [17] introduces a multi-level framework for high fidelity 3D reconstruction of clothed human. It uses an additional image translation net to predict normal maps from original color images. The predicted normal maps enable it to reconstruct more geometry details, such as clothing folds. Moreover, a fine-level is used in PIFuHD to recover more subtle details from the high resolution input images.

For multi-view human reconstruction, PIFu uses a naive average pooling operation for multi-view feature fusion, which is not efficient enough to fuse the geometry details that observed in the multi-view input images. To tackle this problem, [18] uses self-attention for multi-view feature fusion and get better reconstruction results. However, [18] uses SMPL as the geometry prior to solve the occlusion problem in multi-person reconstruction, which not only makes the reconstruction results might be pixel-misaligned, but also makes it unable to reconstruct the human cases with loose clothes, such as long dress. In contrast, without using any geometry prior, we present a pixel-aligned spatial transformer for multi-view feature fusion, enabling us to produce pixel-aligned highly detailed reconstruction results.

View Synthesis. Many works [1], [19], [20] use the traditional image-based rendering or view synthesis pipeline for novel view rendering, i.e. proxy geometry reconstruction-warping-blending. To bridge the gap between reconstruction and rendering, [4] presents a point cloud based method to improve multi-view stereo algorithm for more realistic free view synthesis (FVV). Benefit from the significant research progress of deep learning in recent years, some works [1], [3] use neural networks to blend the novel views from the warped source views. However, these warping-based works need dense camera views as input to warp the source views to the novel view. If the input camera views are highly sparse, the performances of this classic method will degrade dramatically as the wide camera baselines will cause severe occlusion problems.

More recently, volume rendering is another method to achieve photo-realistic rendering. It uses volumes to represent the shape and appearance of a scene. Multi-plane images (MPIs) [21] is one of the most promising ways for this volumetric representation, which computes a separate RGB α image for each depth plane. The α channel and the RGB channels represent the shape and appearance of the scene respectively. Based on the MPIs-representation, [2]

introduces a soft 3D representation of the scene geometry. This representation enables it to handle the depth uncertainty of the scene. Benefit from the significant research progress on neural networks, [22], [23] use neural networks to predict the MPIs for each input views. Another promising research direction for volume rendering is neural radiance fields (NeRF) [9], which uses a multi-layer perceptron (MLP) to represent the density and color fields of a scene and thus it is well-suited for differentiable rendering. However, both MPIs-based and NeRF-based works need dense camera views as input and always need to train or fine-tune a separate network of each scene. For human rendering on sparse views, [5] uses latent codes that anchored on SMPL vertices to integrate observations from a multi-view video, thus enabling it to reconstruct and render humans from sparse views. However, [5] is only able to render humans with pure clothes. When human performers wear clothes with complex patterns, its rendering quality is still very low as the SMPL models do not contain any geometry details. Besides, it needs to train a separate network for each human, which is extremely time-consuming. In our work, we introduce a new general framework for the high quality rendering of challenging human performers with complex clothes using sparse views.

3 APPROACH

Given a sparse set of challenging human views as input, the goal of our method is to render high quality images on novel views. For 4D human rendering, our system pipeline can be divided into three parts: 1) a reconstruction net with pixel-aligned spatial transformer for highly detailed initial reconstruction (Sec.??), 2) a skeleton-based tracking method for more robust and coherent 4D human reconstruction (Sec.3.2), and 3) a render net with geometry-guided pixel-wise feature integration for novel view human rendering (Sec.3.3). Note that the tracking step is only possible in 4D human reconstruction, so for static human rendering, we will use the reconstructed meshes from the reconstruction net as the geometry input of the render net.

3.1 Pixel-aligned reconstruction with spatial transformer

PIFu [16] introduces a pixel-aligned implicit function to reconstruct the underlining 3D human geometry from a single or multi-view images. The proposed pixel-aligned implicit function consists of a convolutional image encoder g and a continuous implicit function f that represented by a multi-layer perceptron. Concretely, the human surface is defined as

$$f(g(I(x)), z(X)) = s : s \in \mathbb{R} \quad (1)$$

where X is the given 3D point, $x = \pi(X)$ is its orthogonal 2D projection, $g(I(x))$ is the bilinear sampled image feature at x . During the inference, 3D space is uniformly sampled to infer the occupancy and the final iso-surface is extracted with a threshold of 0.5 using marching cube algorithm.

To achieve high-fidelity 3D reconstruction of clothed human from a single image, recovering detailed information such as clothing folds, PIFuHD [17] proposes a coarse-to-fine framework for 3D clothed human reconstruction

using images with resolution of 1024×1024 . It uses an additional network to predict normal maps from the input color images. Compared with PIFu, the predicted normal maps enable it to recover more details as the geometry information in normal maps is more explicit. Moreover, a fine-level is used in PIFuHD to recover details from high resolution images. Specifically, the fine level can be denoted as

$$f^H(g^H(I_H, F_H, B_H, x_H), \Omega(X)) = s : s \in \mathbb{R} \quad (2)$$

where I_H, F_H, B_H are the input color images and the predicted front and back normal maps at resolution of 1024×1024 . $\Omega(X)$ is the feature extracted from the coarse level.

For multi-view reconstruction, PIFu [16] uses a naive average pooling operation to fuse multi-view features. This average pooling operation is not efficient enough for fusing the geometry details that observed in the input multi-view images as it regard each view equally. But in fact, for each 3D point in world space, different views should have different weights for the occupancy estimation of the 3D point. [18] uses human shape and pose prior SMPL [6] for multi-person reconstruction using sparse views, which makes it capable of solving the occlusion problems caused by the interaction of multi-human. However, the SMPL models do not have any geometry details, which will cause two problems: 1) the reconstruction results might be pixel-misaligned, 2) it will be difficult to reconstruct humans with loose clothes, such as long dress.

To achieve the goal of high quality human rendering, highly detailed reconstruction of humans is essential. The key to this reconstruction problem is how to preserve the geometry details that observed in the input multi-view images. For this end, we propose a pixel-aligned spatial transformer in the reconstruction net for highly detailed human reconstruction. See Fig.2 for an illustration.

Following [17], we firstly predict frontal normal maps from color images, and encode each view’s color image and normal map using a Hourglass encoder g . Our observation is that in multi-view reconstruction, the coarse level network in [17] is enough to reconstruct high-frequency details with frontal normal maps as input. So, for memory efficiency, we only use a single level for reconstruction.

To efficiently preserve the geometry details that observed in the input views, we use a spatial transformer to calculate the correlations between input multi-view pixel-aligned features. Specifically, for a 3D point X , given N views encoded features, we will stack them together to get $\Phi_{mv} \in \mathbb{R}^{N \times D}$, where D is the feature dimensions. And then we embed it with three learnable different linear layers: $\Phi_q = \Phi_{mv} W_q$, $\Phi_k = \Phi_{mv} W_k$, $\Phi_v = \Phi_{mv} W_v$, where $W_q, W_k, W_v \in \mathbb{R}^{D \times d_k}$ and $\Phi_q, \Phi_k, \Phi_v \in \mathbb{R}^{N \times d_k}$. d_k is the embedded feature dimension. Then, a spatial transformer will be applied:

$$\Phi_{mv_att} = Transformer(\Phi_q, \Phi_k, \Phi_v) = softmax\left(\frac{\Phi_q \Phi_k^T}{\sqrt{d_k}}\right) \Phi_v \quad (3)$$

where $\Phi_{mv_att} \in \mathbb{R}^{N \times d_k}$ is the transformer-aware multi-view features. To counter the gradient vanishing problem causing by the softmax operation, we scale the dot-product

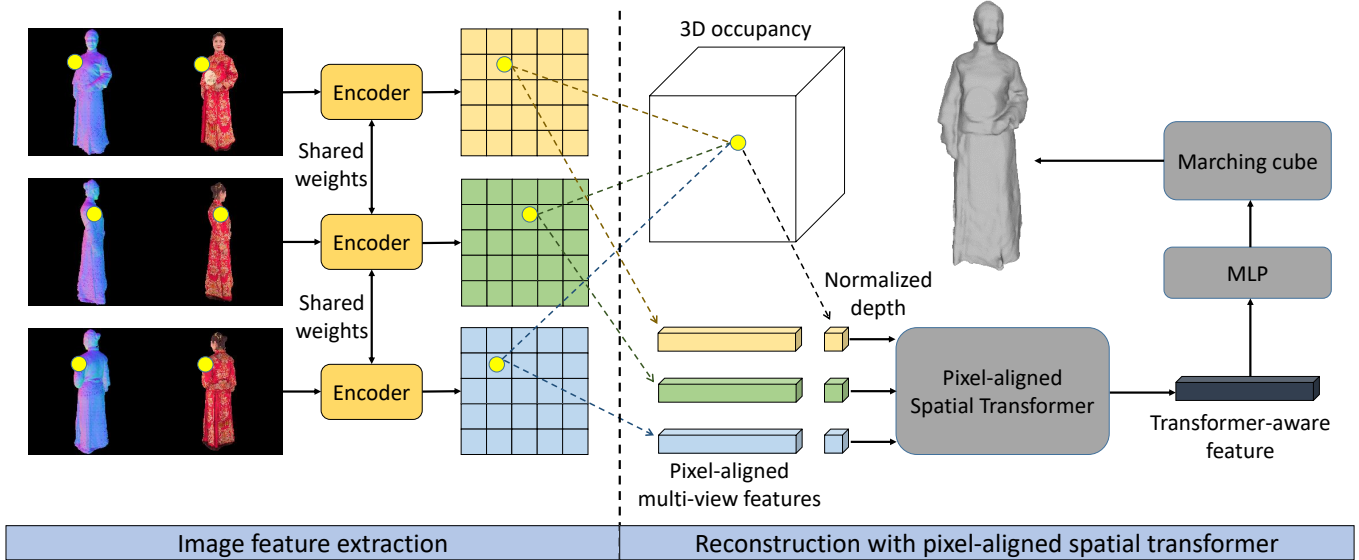


Fig. 2. **Architecture of our reconstruction net.** For memory efficiency, we only use a single level for reconstruction. The pixel-aligned spatial transformer enable us to preserve the geometry details that observed in the input views, resulting in highly detailed reconstruction. Our framework doesn't use any geometry prior, so our reconstruction results are fully pixel-aligned.

operation by $\frac{1}{\sqrt{d_k}}$. Different from the feature before transformer calculation, which only contains the geometry details observed in a single view, the transformer-aware feature contains all the geometry details that observed in multi-view images. Compared with the average pooling operation in [16], the transformer-based fusion operation calculates the correlations between the multi-view features, which provides a high-level information for fusion, allowing the network to preserve more geometry details.

To query the depth value of point X with the encoded features, we need to normalize the depth value for each view. Given multi-view human images and the corresponding calibrated camera parameters as input, we will estimate each view's human 2D skeleton using Openpose [24], and then obtain 3D skeleton $S_w \in \mathbb{R}^{3 \times J}$ in world space through triangulation. J is the number of joints. We use the hip position $H_w \in \mathbb{R}^3$ and neck position $N_w \in \mathbb{R}^3$ to normalize the depth. Specifically,

$$H_c^i = R_i H_w + t_i = (H_{c_x}^i, H_{c_y}^i, H_{c_z}^i) \quad (4)$$

$$X_c^i = R_i X + t_i = (X_{c_x}^i, X_{c_y}^i, X_{c_z}^i) \quad (5)$$

$$z_i(X_{c_z}^i) = \frac{X_{c_z}^i - H_{c_z}^i}{\lambda \|H_w - N_w\|_2} \quad (6)$$

where H_c^i, X_c^i is the hip position and the point X position in view i 's camera space respectively. R_i, t_i is camera i 's rotation and translation. λ is a constant value to make sure the normalized depth always lies in $(0, 1)$, and we set it to $4\sqrt{3}$ in all our experiments.

Finally, we use a multi-layer perceptron to predict the 3D occupancy and use marching cube algorithm to extract the surface from the predicted occupancy, resulting in the final reconstructed mesh.

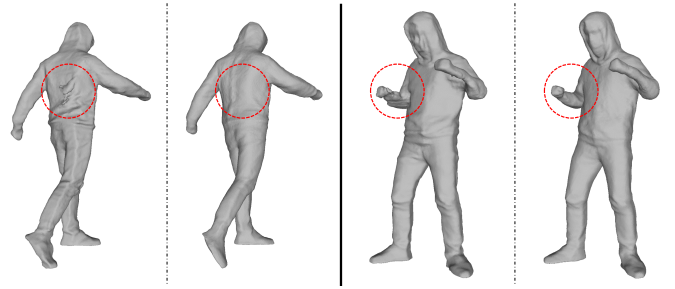


Fig. 3. This figure shows the effect of tracking. The first column shows the reconstruction artifact caused by normal maps inconsistency across views. The third column shows the reconstruction artifact caused by occlusion problems. The second and fourth columns show the results after tracking, which solves the artifacts while maintaining the geometry details.

3.2 Tracking

With a sparse set of camera views as input, some parts of human bodies can only be observed in one input view, or even invisible in some frames, which causes severe occlusion problems, resulting in reconstruction failures in these parts, such as the arms (third column in Fig.3). Moreover, the predicted normal maps might be inconsistent across views, which will also cause reconstruction artifacts (first column in Fig.3). To solve the reconstruction failures caused by occlusion or inconsistency while maintaining the geometry details, we present a tracking method for 4D reconstruction. Our tracking method mainly includes three steps: Skeleton tracking & Animation, Rigid Refinement and Deformation.

Skeleton tracking & Animation. For 4D reconstruction, we firstly extract the 3D skeleton and reconstruct the mesh for each frame using the method introduced in section ??, resulting in skeleton sequence $S = \{s^1, \dots, s^F\}$ and mesh sequence $M_{recon} = \{m_{recon}^1, \dots, m_{recon}^F\}$. F is the number of frames. And then we will select a frame c as the canonical

frame and rig the frame’s 3D skeleton s^c to the reconstructed mesh m_{recon}^c using [25]. After rigging, we will get blending weights, enabling us to animate the canonical mesh using 3D skeletons through linear blend skinning. To animate the canonical mesh to another frame f , we solve an inverse kinematic problem between the canonical skeleton s^c and frame f ’s skeleton s^f :

$$E_{IK}(\theta_{ani}^f) = \|s^c(\theta_{ani}^f) - s^f\|_1 \quad (7)$$

where $\theta_{ani}^f \in \mathbb{R}^{J \times 3}$ is the kinematic parameters of frame f and is initialized as $\mathbf{0}$. J is the number of joints. Each row i in θ_{ani}^f is the rotation vector of joint i . $s^c(\theta_{ani}^f)$ is the animated canonical skeleton. After calculating each frame’s kinematic parameters, we will animate the canonical mesh using the calculated parameters and the rigged blending weights, resulting in mesh sequence $M_{ani} = \{m_{ani}^1, \dots, m_{ani}^F\}$.

Rigid Refinement. After animation, the animated mesh and the reconstructed mesh might be misaligned, which is caused by the skeleton estimation errors. In order to relieve this misalignment, we will refine each frame’s kinematic parameters by solving the energy function E_{refine} :

$$E_{refine}(\theta_{refine}^f) = Dist(m_{refine}^f - m_{recon}^f) \quad (8)$$

$$m_{refine}^f = m_{recon}^c(\theta_{refine}^f) \quad (9)$$

where θ_{refine}^f is the refined kinematic parameters and is initialized as θ_{ani}^f . m_{refine}^f is the animated refined mesh using the refined parameters. $Dist$ is a function that calculates the distance between the refined mesh and reconstructed mesh, i.e. for every vertex in the refined mesh, we found its nearest neighbor in the reconstructed mesh and calculate their euclidean distance and add the distances for all the vertices. After the rigid refinement, we will get a refined mesh sequence $M_{refine} = \{m_{refine}^1, \dots, m_{refine}^F\}$.

Deformation. After animation and refinement, the tracked mesh sequence M_{refine} doesn’t contain the geometry details for each frame. We will apply a non-rigid deformation to the refined mesh sequence M_{refine} to recover each frame’s geometry details.

$$E_{deform}(\delta^f) = (m_{deform}^f - m_{recon}^f) + \lambda Reg(m_{deform}^f) \quad (10)$$

$$m_{deform}^f = m_{refine}^f(\delta^f) \quad (11)$$

where $\delta \in \mathbb{R}^{N \times 3}$ is the translation for the vertices of the mesh m_{refine}^f . N is the number of vertices. $(m_{deform}^f - m_{recon}^f) \in \mathbb{R}^{N \times 3}$ is the distance between each vertex of m_{deform}^f and its nearest neighbor in m_{recon}^f . $Reg(m_{deform}^f) \in \mathbb{R}^{E \times 3}$ is the regular term: for each edge in mesh m_{deform}^f , we calculate the translation difference of the two vertices in the edge. E is the number of edges. λ is a hyper-parameter that balances the deform term and regular term. We set it to 100 in all our experiments. We solve all the energy functions using Gaussian-Newton solver. After deformation, we get a deformed mesh sequence $M_{deform} = \{m_{deform}^1, \dots, m_{deform}^F\}$. Compared with the reconstructed mesh sequence M_{recon} , M_{deform}

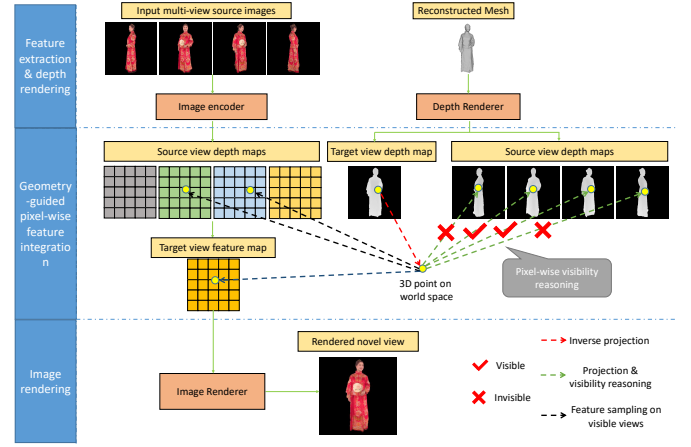


Fig. 4. **Architecture of our render net.** The geometry-guided feature integration capable us to solve the severe occlusion problems caused by the sparsity of input views, resulting in high quality novel view rendering.

solves the artifacts caused by occlusion and normal maps inconsistency while maintaining the geometry details (second and fourth column in Fig.3). For 4D rendering, we will use the deformed mesh sequence as the geometry input for novel view rendering.

3.3 Novel View Rendering

Given a sparse set of input images $\{I_0, \dots, I_N\}$, the corresponding calibrated camera parameters and the reconstructed meshes, we use a render net to render high quality novel view images of human performers. To achieve the goal of high quality rendering, the core is to solve the occlusion problems caused by the sparsity of input views. For this end, we present a geometry-guided pixel-wise feature integration method in the render net for solving the occlusions. The architecture of render net is shown in Fig.4. In summary, we use a encode-integration-render framework for novel view rendering, which mainly consists of three parts: 1) encoding each input image to feature space using an encoder net e , 2) pixel-wise visibility reasoning and feature integration using the reconstructed human geometry, 3) render the novel view image using a render net r .

Image encoding. For each input image $I_n \in \mathbb{R}^{H \times W \times 3}$, we firstly encode it to a high-dimensional feature space and get feature map $F_n = e(I_n) \in \mathbb{R}^{H \times W \times D}$ at the same resolution. Following [26], the encoder e uses a Res-UNet architecture, where the encoding part is an ImageNet-pretrained ResNet [27] and the decoding part upsamples the feature map using nearest-neighbor interpolation, concatenating it with the corresponding feature map (of the same resolution) from the encoding part.

Geometry-guided pixel-wise feature integration An essential step for novel view rendering is to map the source views to the novel view and traditional IBR methods always use warping operation to map the source views to the novel view. We argue that the warping operation will warp the pixels or areas that are not visible in the novel view, resulting in rendering artifacts or blurring,

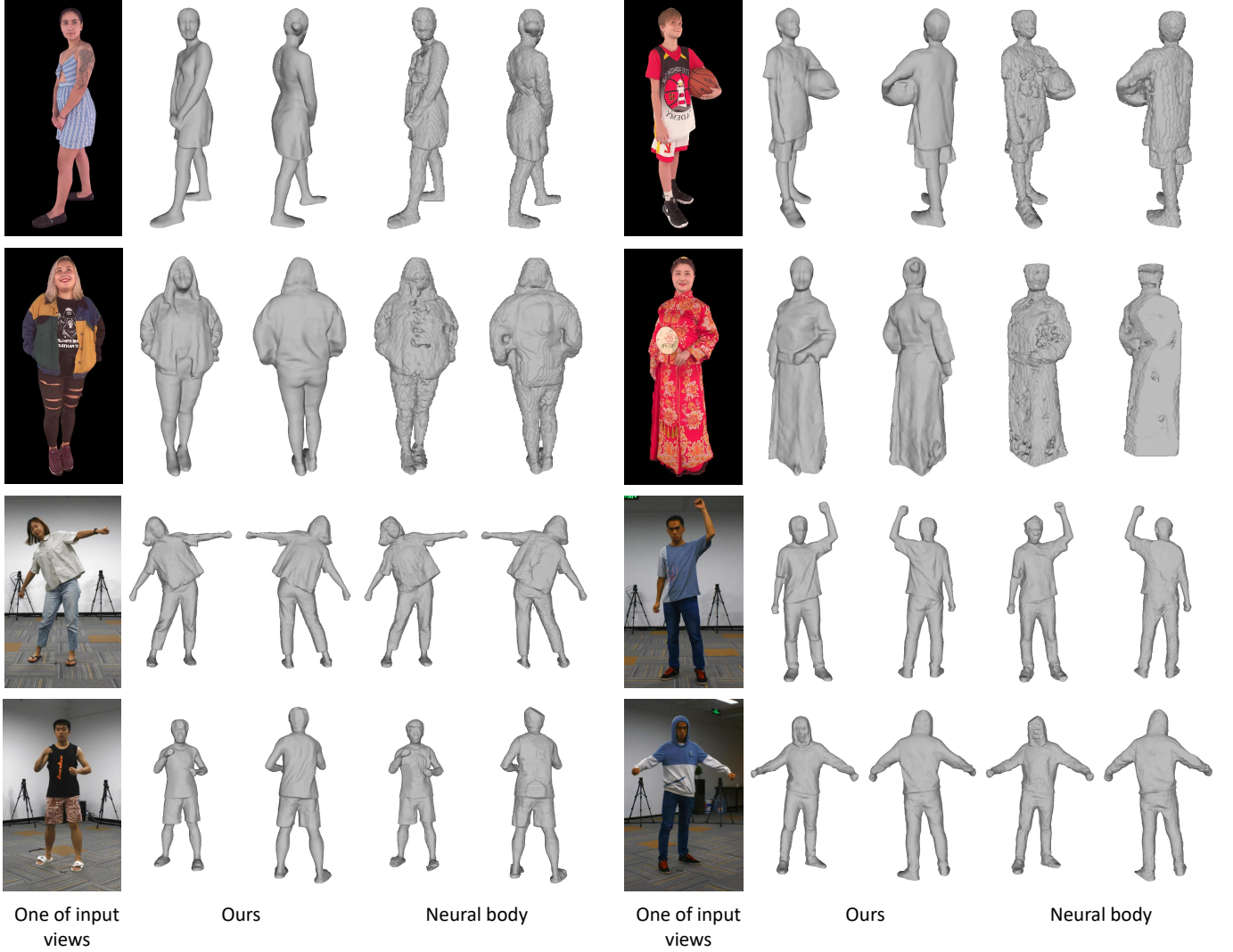


Fig. 5. **Qualitative results of reconstruction.** The top two rows are the results on twindom dataset, with 6 views as input. The bottom two rows are the results on real-world data, with 8 views as input. We strongly recommend the readers to zoom the pages for a better visualization of the reconstructed details.

thus the warping operation is not suitable for solving the occlusion problems. To render high quality novel view images from sparse views, the core is solving the occlusion problems caused by the sparsity of views. For each pixel in a novel view, the visible input views is different. So we perform visibility reasoning and get the visible source views for each pixel in the novel view. And then only integrate features from visible source views to the novel view pixel, the source views that are not visible will be abandoned. Concretely, given input views' calibrated camera parameters (including intrinsic and extrinsic parameters) $\{C_1, \dots, C_N\}$, the novel view camera C_{novel} and the reconstructed human mesh, we will render depth maps of the input views $\{D_1, \dots, D_N\}$ and novel views D_{novel} using OpenGL or Taichi. And then, for each pixel $p \in \mathbb{R}^2$ with valid depth value ($d_{render} > 0$) in the novel view, we will unproject it to the world space, getting point $P \in \mathbb{R}^3$, and then reproject to each input view's image space using the corresponding cameras, getting the reprojected pixel and depth and rendered depth in each view

$\{(p_{reproj_1}, d_{reproj_1}, d_{render_1}), \dots, (p_{reproj_N}, d_{reproj_N}, d_{render_N})\}$, i.e.

$$(p_{reproj_n}, d_{reproj_n}, d_{render_n}) = C_n(C_{novel}^{-1}(p, d_{render})) \quad (12)$$

where $d_{render_n} = D_n(p_{reproj_n})$. If the difference between the rendered depth and reprojected depth is lower than a threshold, we will regard view n is visible for pixel p :

$$|d_{render_n} - d_{reproj_n}| < \lambda \cdot \min(d_{render_n}, d_{reproj_n}) \quad (13)$$

where λ is a hyper-parameter and we set it to 0.01 in all our experiments.

After the visibility reasoning, we will sample features from all the visible views' using bilinear sampling. i.e. $f_n = F_n(p_{reproj_n})$, and getting $\{f_1, \dots, f_K\}$, where K is the number of visible source views for pixel p . And then, a simple direction average operation will be performed to integrate source view features to the novel view pixel:

$$f_{fusion} = \frac{1}{W} \sum_{k=1}^K \max(0, \cos\langle dir_{novel}, dir_k \rangle) \cdot f_k \quad (14)$$

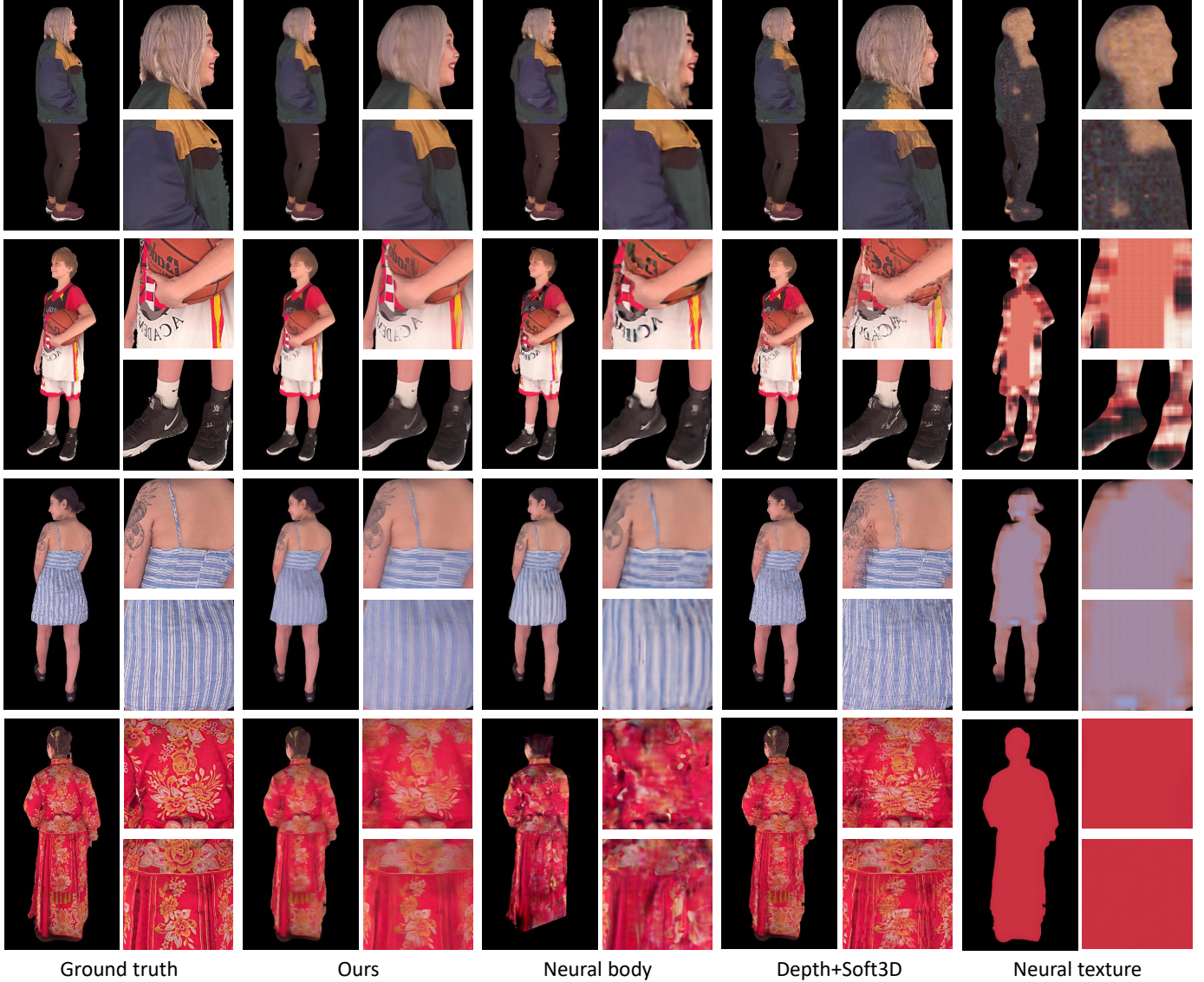


Fig. 6. **Novel view rendering on Twindom dataset.** We use 6 views as input. Results show that our method significantly outperforms all other methods qualitatively, especially in the areas that have complex details.

where dir_{novel}, dir_k are the novel view direction and the visible source view k 's direction respectively. The fused novel view feature is divided by $W = \sum_{k=1}^K \max(0, \cos\langle dir_{novel}, dir_k \rangle)$ for normalization.

Novel view rendering. After getting the feature map F_{novel} of the novel view, we will use a render net r to render the novel view's color image i.e. $I_{novel} = r(F_{novel})$. The architecture of render net is a stacked U-Net, where each stack L learns the residual of F_{novel} , i.e. $r(F_{novel}) = r^L(F_{novel} + r^{L-1}(F_{novel} + r^{L-2}(\dots)))$.

4 EXPERIMENTS

4.1 Training

Dataset: We collect 1700 high quality textured human meshes from Twindom as a large scale dataset for the training and evaluation of our model. The collected models have a wide range of clothing, poses and shapes. We randomly

split the models into a training set of 1500 subjects and a testing set of 200 subjects.

Reconstruction net training For each subject in dataset, we generate 360 virtual perspective cameras in yaw axis (1 camera for each degree) and each camera has a random pitch angle. And then we render 360 images at a resolution of 512×512 using Taichi. During training, we randomly pick 4 views over the 360 images as input for each iteration. We use Adam optimizer with a learning rate of 1×10^{-4} and train the reconstruction net for nearly 300000 iterations for convergence. The training procedure costs 3 days with a batch size of 1 in a single Nvidia TitanXp GPU.

Render net training The render net needs reconstructed meshes as input, but we didn't use the ground truth geometry. Instead, we randomly picking 5 views over the 360 images and use the reconstruction net to generate a coarse mesh for each subject. With coarse meshes as in-

TABLE 2

Quantitative rendering results on Twindom dataset. "NB" means neural body. "D+S3D" means Soft3D with our depth maps as input. "NT" means neural texture. For each model, we use 6 views as input and 30 views for evaluation.

	LPIPS (lower better)				SSIM (higher better)				PSNR (higher better)			
	Ours	NB [5]	D+S3D [2]	NT [10]	Ours	NB [5]	D+S3D [2]	NT [10]	Ours	NB [5]	D+S3D [2]	NT [10]
Model1	0.1455	0.2660	0.1802	0.2949	0.876	0.842	0.831	0.790	25.32	24.63	23.84	22.96
Model2	0.1961	0.2894	0.2516	0.3914	0.782	0.731	0.701	0.612	17.53	17.81	16.26	11.23
Model3	0.1217	0.2132	0.1788	0.3191	0.865	0.832	0.793	0.712	21.75	21.81	19.49	13.37
Model4	0.2296	0.4246	0.2651	0.4377	0.610	0.469	0.560	0.501	18.53	14.35	17.52	15.16
Model5	0.1304	0.2743	0.1723	0.3035	0.794	0.745	0.739	0.696	21.76	21.33	20.30	17.66
Average	0.1647	0.2931	0.2096	0.3493	0.785	0.724	0.725	0.662	20.98	20.03	19.48	16.08

TABLE 3

Quantitative reconstruction results on twindom dataset. For each model, we use 6 views for reconstruction. Our reconstruction results outperform neural body by a large margin.

	P2S		Chamfer	
	Ours	Neural body [5]	Ours	Neural body [5]
Model1	0.1866	0.9299	0.1968	0.7030
Model2	0.2604	0.8902	0.3817	0.6753
Model3	0.1718	0.6639	0.1840	0.5410
Model4	0.3858	1.8421	0.4070	1.5791
Model5	0.1660	0.6104	0.1794	0.5164
Average	0.2698	0.8030	0.2341	0.9873

put, the render net will have greater generalization ability and have more robust performances. We use the generated perspective cameras to render 360 images and depth maps at a higher resolution of 1024×1024 for each subject in our dataset. We divide the yaw axis degrees into 6 parts, each parts has a range of 60 degrees. During training, we randomly pick 1 views in each part, resulting in 6 images as input and then randomly select 1 view as the novel view and other views are source views. We use Adam optimizer with a learning rate of 1×10^{-4} and train for nearly 400000 iterations for convergence. The training procedure costs nearly 2 days with a batch size of 1 using a single Nvidia RTX3090 GPU.

4.2 Evaluation Settings

In this section, we will introduce our evaluation metrics, compared methods and the settings for each compared method. The evaluation will be performed both on static human performers (synthetic data) and dynamic human performers (real-world data). We highly recommend readers to refer to the website for a better visualization of the reconstruction and rendering results of our methods.

Metrics. For reconstruction, we use Chamfer distance and Point-to-Surface distance (P2S) for quantitative evaluation. For rendering, we will quantitatively evaluate our method using three most widely used metrics: peak signal-to-noise ratio (PSNR), structural similarity index (SSIM) and learned perceptual image patch similarity (LPIPS).

Compared methods. We compare our method with both general and scene/human-specific rendering methods [2], [5], [10]. 1) Neural texture [10] introduces differentiable latent neural texture maps for novel view rendering. It needs to train a separate network for each scene or human. Note

that to evaluate [10] on dynamic humans, topological consistent reconstruction of human performers is necessary. The deformed sequence M_{deform} after tracking in our method is a topological consistent mesh sequence, so we use it as the input meshes to evaluate [10]. 2) Soft3D [2] is a MPI-based method for view synthesis, which uses multi-plane images(MPI) to handle the uncertainty of depth maps. It is a general view synthesis method that doesn't need to train any network. Note that [2] doesn't use any geometry prior, so it needs to use MPI to estimate an initial depth map for each input image, which is extremely coarse, making the quality of synthesis images very low. For fairness, we will use the rendered depth maps in our method as the initial depth maps for an additional input of [2], which improves its performance. 3) Neural body [5] proposes a NeRF-based implicit neural representation for human novel view rendering, it needs to train a separate network for each human. Note that reconstruction results are only available on neural body [5], so we will perform comparisons with it for reconstruction evaluation.

4.3 Results on static human rendering (synthetic data)

We select 5 models in the testing set of Twindom for the evaluation on synthetic data. For each model, we render 36 images in a circle arrangement at a resolution of 2048×2048 and use 6 uniformly distributed views as input and the remaining 30 views for evaluation. Table 3 shows the quantitative reconstruction comparisons of our method with neural body [5]. For both P2S distance and Chamfer distance, our method outperforms [5] by extremely large margins. Some qualitative reconstruction results are shown on the top two rows of Fig.5. The reconstruction results are produced with only 6 views as input, showing that our method is able to perform highly detailed reconstruction of challenging humans using only a sparse set of camera views.

For novel view rendering, quantitative results are shown in table 2. Our method achieves the best performances among all the methods in LPIPS metric and SSIM metric. Fig.6 shows some qualitative rendering results. The results show that our method is able to rendering high quality images on challenging humans that wear clothes with complex patterns or ware loose clothes such as long dress.

4.4 Results on 4D human rendering (real-world data)

For the evaluation of 4D human rendering, we create a multi-view dataset, which captures 5 dynamic human videos using a multi-camera system that has 24 calibrated

TABLE 4

Quantitative rendering results on our multi-view videos dataset. "NB" means neural body. "D+S3D" means Soft3D with our depth maps as input. "NT" means neural texture. For each frame, we use 8 views as input and 16 views for evaluation. Each sequence has a length of 150 frames.

	LPIPS (lower better)				SSIM (higher better)				PSNR (higher better)			
	Ours	NB [5]	D+S3D [2]	NT [10]	Ours	NB [5]	D+S3D [2]	NT [10]	Ours	NB [5]	D+S3D [2]	NT [10]
Sequence1	0.1455	0.2660	0.1802	0.2949	0.823	0.732	0.722	0.687	24.14	21.05	21.11	17.61
Sequence2	0.1961	0.2894	0.2516	0.3914	0.787	0.659	0.671	0.649	22.36	20.60	19.13	17.11
Sequence3	0.1217	0.2132	0.1788	0.3191	0.887	0.831	0.811	0.790	25.04	22.76	22.10	19.81
Sequence4	0.2296	0.4246	0.2651	0.4377	0.872	0.832	0.797	0.796	26.90	25.35	24.42	22.88
Sequence5	0.1304	0.2723	0.1723	0.3035	0.880	0.822	0.800	0.751	26.47	24.32	23.45	17.59
Average	0.1647	0.2931	0.2096	0.3493	0.850	0.775	0.760	0.735	24.98	22.82	22.04	19.00

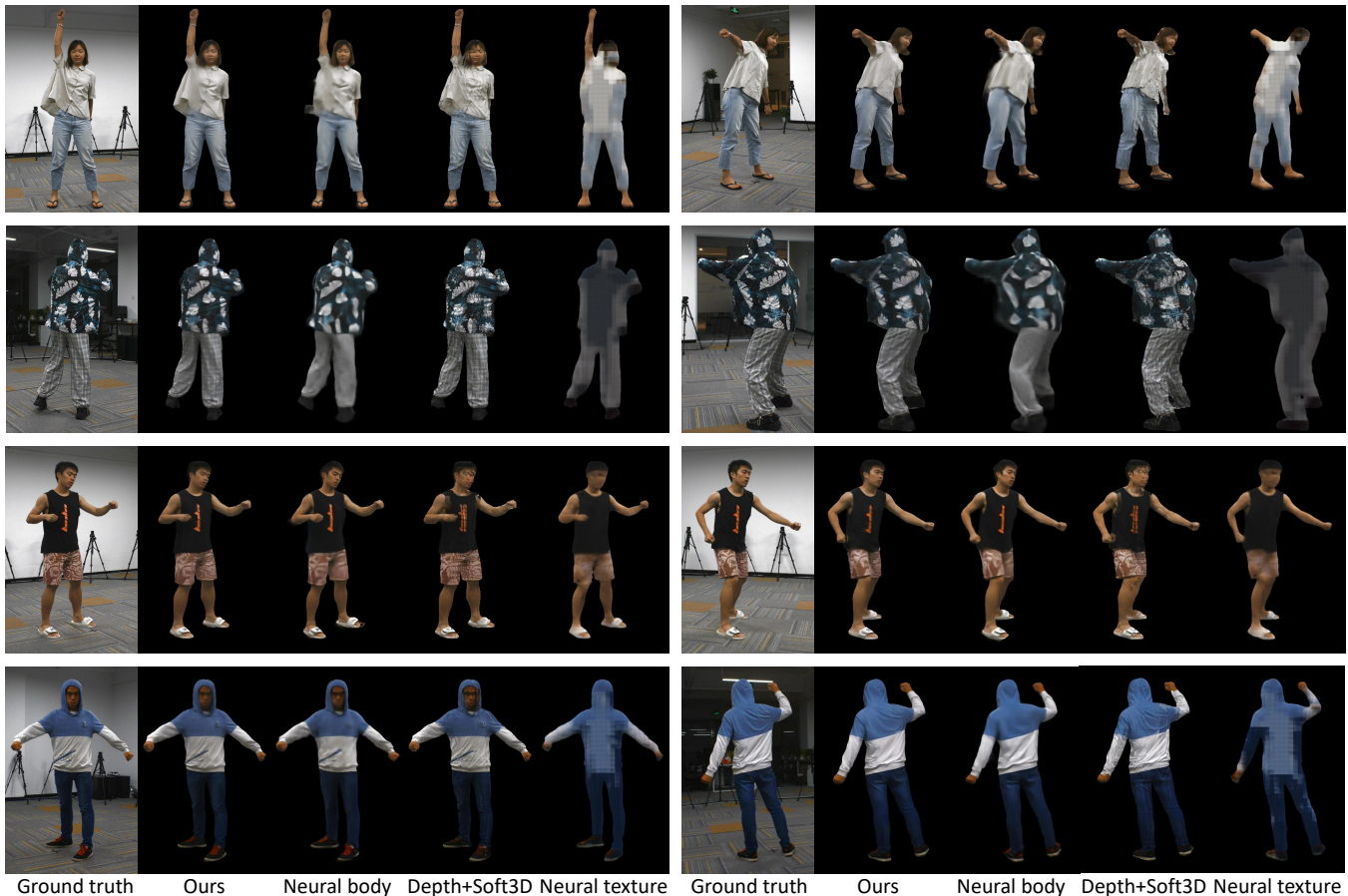


Fig. 7. **Novel view rendering on our captured multi-view videos dataset.** We use 8 views as input. We strongly recommend the readers to zoom the pages for a better visualization of the rendered details.

synchronized cameras in a circle arrangement. In contrast to the dataset of NeuralBody [5], which only captures humans with pure color clothes, our captured human performers wear clothes with complex color patterns or loose clothes. We select 8 uniformly distributed cameras as the source input views and use the remaining 16 cameras for testing. All sequences have a length of 150 frames.

Some qualitative results are shown on the bottom two rows of fig. 2. Compared with neural body, our reconstruction results have more high-frequency details, such as clothing folds. Achieving great performances on real-world data means that the proposed pixel-aligned spatial transformer is robust and efficient.

The quantitative results is shown on table 4. Our method outperforms all other methods on all the measured metrics. Fig.7 illustrates some qualitative results. The novel

views rendered by our method contains more texture details compared with other methods. Benefit from the geometry-guided pixel-wise feature integration, we solve the occlusion problems caused by the sparsity of input views, resulting in the robust high quality rendering on real-world data.

5 CONCLUSION, DISCUSSION AND FUTURE WORKS

In this paper, we introduce HumanIBR, a general method that uses pixel-aligned spatial transformer and geometry-guided pixel-wise feature integration for high quality human reconstruction and rendering using sparse views. Experiments show that our rendering quality significantly outperforms both the general and scene/human-specific methods. Our method demonstrates that high-quality human

rendering in sparse views is possible without any network fine-tuning, which can serve as an important baseline in the area of human rendering.

However, the geometry representation we used are meshes, so the geometry-guided pixel-wise feature integration used in our method is indifferentiable with the reconstructed geometry, making us unable to refine the geometry if we fine-tune our networks. Instead, we can only optimize the parameters in the render net, which will result in blur in the areas that have artifacts. So the fine-tuning operation can not significantly improve the rendering performances, which is an important limitation of our method.

In future, a research direction that is worthy to explore is to use a geometry representation that is differentiable in our framework. For example, we could encode the reconstructed mesh to a volume, and then perform differentiable geometry-guided visibility reasoning for each voxel and finally use volume rendering techniques to render novel views. In this way, the geometry will be differentiable and we will be able to refine the geometry in the procedure of fine-tuning.

REFERENCES

- [1] P. Hedman, J. Philip, T. Price, J.-M. Frahm, G. Drettakis, and G. Brostow, "Deep blending for free-viewpoint image-based rendering," *ACM Transactions on Graphics (TOG)*, vol. 37, no. 6, pp. 1–15, 2018. 1, 1, 2
- [2] E. Penner and L. Zhang, "Soft 3d reconstruction for view synthesis," *ACM Transactions on Graphics (TOG)*, vol. 36, no. 6, pp. 1–11, 2017. 1, 1, 2, 2, 4.2, 4
- [3] G. Riegler and V. Koltun, "Free view synthesis," in *European Conference on Computer Vision*, 2020. 1, 2
- [4] Y. Liu, Q. Dai, and W. Xu, "A point-cloud-based multiview stereo algorithm for free-viewpoint video," *IEEE transactions on visualization and computer graphics*, vol. 16, no. 3, pp. 407–418, 2009. 1, 2
- [5] S. Peng, Y. Zhang, Y. Xu, Q. Wang, Q. Shuai, H. Bao, and X. Zhou, "Neural body: Implicit neural representations with structured latent codes for novel view synthesis of dynamic humans," in *CVPR*, 2021. 1, 1, 1, 2, 2, 3, 4.2, 4.3, 4, 4.4
- [6] M. Loper, N. Mahmood, J. Romero, G. Pons-Moll, and M. J. Black, "Smpl: A skinned multi-person linear model," *ACM transactions on graphics (TOG)*, vol. 34, no. 6, pp. 1–16, 2015. 1, 3.1
- [7] Q. Wang, Z. Wang, K. Genova, P. P. Srinivasan, H. Zhou, J. T. Barron, R. Martin-Brualla, N. Snavely, and T. Funkhouser, "Ibrnet: Learning multi-view image-based rendering," in *Proceedings of the IEEE/CVF Conference on Computer Vision and Pattern Recognition*, 2021, pp. 4690–4699. 1, 1
- [8] A. Yu, V. Ye, M. Tancik, and A. Kanazawa, "pixelNeRF: Neural radiance fields from one or few images," in *CVPR*, 2021. 1, 1
- [9] B. Mildenhall, P. P. Srinivasan, M. Tancik, J. T. Barron, R. Ramamoorthi, and R. Ng, "Nerf: Representing scenes as neural radiance fields for view synthesis," in *European conference on computer vision*. Springer, 2020, pp. 405–421. 1, 2
- [10] J. Thies, M. Zollhöfer, and M. Nießner, "Deferred neural rendering: Image synthesis using neural textures," *ACM Transactions on Graphics (TOG)*, vol. 38, no. 4, pp. 1–12, 2019. 1, 2, 4.2, 4
- [11] Y. Liu, X. Cao, Q. Dai, and W. Xu, "Continuous depth estimation for multi-view stereo," in *2009 IEEE Conference on Computer Vision and Pattern Recognition*. IEEE, 2009, pp. 2121–2128. 2
- [12] A. Collet, M. Chuang, P. Sweeney, D. Gillett, D. Evseev, D. Calabrese, H. Hoppe, A. Kirk, and S. Sullivan, "High-quality streamable free-viewpoint video," *ACM Transactions on Graphics (ToG)*, vol. 34, no. 4, pp. 1–13, 2015. 2
- [13] M. Dou, S. Khamis, Y. Degtyarev, P. Davidson, S. R. Fanello, A. Kowdle, S. O. Escolano, C. Rhemann, D. Kim, J. Taylor *et al.*, "Fusion4d: Real-time performance capture of challenging scenes," *ACM Transactions on Graphics (ToG)*, vol. 35, no. 4, pp. 1–13, 2016. 2
- [14] T. Yu, Z. Zheng, K. Guo, P. Liu, Q. Dai, and Y. Liu, "Function4d: Real-time human volumetric capture from very sparse consumer rgbd sensors," in *Proceedings of the IEEE/CVF Conference on Computer Vision and Pattern Recognition*, 2021, pp. 5746–5756. 2
- [15] K. Guo, F. Xu, T. Yu, X. Liu, Q. Dai, and Y. Liu, "Real-time geometry, albedo, and motion reconstruction using a single rgbd camera," *ACM Transactions on Graphics (ToG)*, vol. 36, no. 4, p. 1, 2017. 2
- [16] S. Saito, Z. Huang, R. Natsume, S. Morishima, A. Kanazawa, and H. Li, "Pifu: Pixel-aligned implicit function for high-resolution clothed human digitization," *arXiv preprint arXiv:1905.05172*, 2019. 2, 3.1, 3.1, 3.1
- [17] S. Saito, T. Simon, J. Saragih, and H. Joo, "Pifuhd: Multi-level pixel-aligned implicit function for high-resolution 3d human digitization," in *Proceedings of the IEEE/CVF Conference on Computer Vision and Pattern Recognition*, 2020, pp. 84–93. 2, 3.1, 3.1
- [18] Y. Zheng, R. Shao, Y. Zhang, T. Yu, Z. Zheng, Q. Dai, and Y. Liu, "Deepmulticap: Performance capture of multiple characters using sparse multiview cameras," *arXiv preprint arXiv:2105.00261*, 2021. 2, 3.1
- [19] G. Chaurasia, S. Duchene, O. Sorkine-Hornung, and G. Drettakis, "Depth synthesis and local warps for plausible image-based navigation," *ACM Transactions on Graphics (TOG)*, vol. 32, no. 3, pp. 1–12, 2013. 2
- [20] J. Thies, M. Zollhöfer, C. Theobalt, M. Stamminger, and M. Nießner, "Ignor: Image-guided neural object rendering," *arXiv preprint arXiv:1811.10720*, 2018. 2
- [21] T. Zhou, R. Tucker, J. Flynn, G. Fyffe, and N. Snavely, "Stereo magnification: Learning view synthesis using multiplane images," *arXiv preprint arXiv:1805.09817*, 2018. 2
- [22] B. Mildenhall, P. P. Srinivasan, R. Ortiz-Cayon, N. K. Kalantari, R. Ramamoorthi, R. Ng, and A. Kar, "Local light field fusion: Practical view synthesis with prescriptive sampling guidelines," *ACM Transactions on Graphics (TOG)*, vol. 38, no. 4, pp. 1–14, 2019. 2
- [23] J. Flynn, M. Broxton, P. Debevec, M. DuVall, G. Fyffe, R. Overbeck, N. Snavely, and R. Tucker, "Deepview: View synthesis with learned gradient descent," in *Proceedings of the IEEE/CVF Conference on Computer Vision and Pattern Recognition*, 2019, pp. 2367–2376. 2
- [24] Z. Cao, G. Hidalgo, T. Simon, S.-E. Wei, and Y. Sheikh, "Openpose: realtime multi-person 2d pose estimation using part affinity fields," *IEEE transactions on pattern analysis and machine intelligence*, vol. 43, no. 1, pp. 172–186, 2019. 3.1
- [25] I. Baran and J. Popović, "Automatic rigging and animation of 3d characters," *ACM Transactions on graphics (TOG)*, vol. 26, no. 3, pp. 72–es, 2007. 3.2
- [26] G. Riegler and V. Koltun, "Stable view synthesis," in *Proceedings of the IEEE Conference on Computer Vision and Pattern Recognition*, 2021. 3.3
- [27] K. He, X. Zhang, S. Ren, and J. Sun, "Deep residual learning for image recognition," in *Proceedings of the IEEE conference on computer vision and pattern recognition*, 2016, pp. 770–778. 3.3